Microwave Scattering Model for Grass Blade Structures

James M. Stiles, Kamal Sarabandi, *Senior Member, IEEE,* and Fawwaz T. Ulaby, *Fellow, IEEE*

Abstract—**In this paper, the electromagnetic scattering solution for a grass blade with complex cross-section geometry is considered. It is assumed that the blade cross section is electrically small, but its length is large compared to the incident wavelength. In a recent study it has been shown that the scattering solution for such problems, in the form of a polarizability tensor, can be obtained using the low-frequency approximation in conjunction with the method of moments. In addition, the study shows that the relationship between the polarizability tensor of a dielectric cylinder and its dielectric constant can be approximated by a simple algebraic expression. The results of this study are used to show that this algebraic approximation is valid also for cylinders with cross sections the shape of grass blades, providing that proper values are selected for each of three constants appearing in the expression. These constants are dependent on cylinder shape, and if the relationship between the constants and the three parameters describing a grass blade shape can be determined, an algebraic approximation relating polarizability tensor to blade shape, as well as dielectric constant, can be formed. Since the elements of the polarizability tensor are dependent on only these parameters, this algebraic approximation can replace the cumbersome method of moments model. The moment method model is therefore used to generate a small but representative set of polarizability tensor data over the range of values commonly observed in nature. A conjugate gradient method is then implemented to correctly determine the three constants of the algebraic approximation for each blade shape. A third-order polynomial fit to the data is then determined for each constant, thus providing a complete analytic replacement to the numerical (moment method) scattering model. Comparisons of this approximation to the numerical model show an average error of less than 3%.**

I. Introduction

Scattering models of random media such as vegetation canopies require knowledge of scattering behavior of the individual vegetation constituents. To obtain efficient scattering formulations for the constituents such as branches, leaves, needles, or stems the structure of these particles are usually modeled by simple canonical geometries, such as circular cylinders or discs [12]. As a result, the particles can be characterized by a few specific geometric parameters, such as length, diameter, or thickness. In addition, scatterers with simple geometries often are amenable to analytic scattering solutions. Due to the random nature of vegetation canopies, scattering formulations for such media are quite complex, thus the two characteristics of simple geometric specification and analytical scattering formulations are highly desirable to provide a tractable vegetation scattering solution.

However, some structural characteristics not reflected in the simplified geometry can significantly affect the scattered response of a given vegetation constituent. That is, oversimplification can degrade the fidelity and accuracy of a canopy scattering model. To provide a greater degree of model accuracy, other physical aspects of these vegetation constituents may be considered, such as blade curvature, branch roughness, or dielectric inhomogeneity [6], [7]. For example, the constituents of a grass plant, such as stems and grass blades, can be modeled as long thin circular dielectric cylinders. The cross sections of grass blades, however, are far from circular. As will be shown, the scattering response of the actual shape is significantly different from that of an equivalent circular cylinder. In addition, a radiative transfer [9]–[11] canopy scattering model demonstrates the resulting discrepancies in backscattering coefficients predicted using the circular, rather than the actual grass blade geometries.

The scattering matrix of electrically thin cylinders with arbitrary cross sections can be determined only with numerical methods and can be expressed in terms of a polarizability tensor. Such is the case for grass blade elements, however, the numeric specification of grass blade shape, along with the numeric scattering solution, are contrary to the desired characteristics described earlier. Thus, the ideal solution would define the blade shape with a few geometric parameters, provide an analytic scattering solution which is a function of these parameters, yet also comprehend and account for the complex blade geometries which affect scattering response.

This is achieved by first approximating the general shape of a grass blade with a collection of geometric parameters, and then limiting the domain of these parameters to those found in nature. The polarizability tenors are obtained numerically for a representative collection of grass blade shapes located throughout this parameter domain, then an analytic function is determined which matches the numeric data and thus approximates the complex polarizability tensor values across the entire domain of shape parameters.

II. Grass Blade Geometry

The fine geometry exhibited by most grass blades occurring in nature can be approximated by a set of five description parameters as shown in Fig. 1. These five parameters, thickness t, width w, blade angle θ, radius of curvature r, and blade length l can be combined to produce five new independent parameters, two of which describe the size of the blade while

Manuscript received September 1, 1992; revised May 3, 1993. This work was supported by NASA Contract NAGW-1101 and by the Jet Propulsion Laboratory under Contract JPL-958438.

The authors are with the Radiation Laboratory, Department of Electrical Engineering and Computer Science, University of Michigan, Ann Arbor, MI 48109-2122.

IEEE Log Number 9210716.

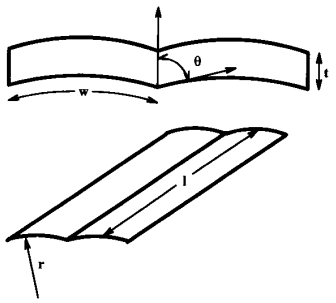

Fig. 1. Diagram of grass blade geometry including blade cross section (showing width w, thickness t, and blade angle θ) and overhead view (showing radius of curvature r and length l).

TABLE I
THE FIVE PARAMETERS DESCRIBING BLADE GEOMETRY, INCLUDING TWO PARAMETERS (LENGTH l, AND AREA A) WHICH SPECIFY BLADE SIZE, AND THREE DIMENSIONLESS PARAMETERS (ASPECT RATIO a, CURVATURE v, AND BLADE ANGLE θ) WHICH SPECIFY SHAPE

parameter	symbol	expression
Area	A	$\approx 2tw$
Length	l	l
Aspect Ratio	a	$t/(2w)$
Curvature	v	w/r
Blade Angle	θ	θ

the other three describe its shape. The first two of these parameters, as shown in Table I, are the cross-sectional area A and blade length l, which together specify the blade size. The three remaining parameters are dimensionless quantities, and thus specify only the blade shape. The first, aspect ratio a, is defined as the ratio of blade thickness to blade width. The second parameter, curvature v, is the arc angle in radians of the arc formed by the curvature of the blade on either side of the center rib. The final parameter, blade angle θ, is the angle formed by the vector normal to the grass blade surface at the center rib, and the vector tangent to the blade curvature at the center rib. In addition, for purposes of the scattering formulation, the grass blades are assumed to be both long and thin, such that $2w \ll \lambda$ and $l \gg w$.

III. SCATTERING FORMULATION

Given these blade parameters and assumptions, a formulation is required to accurately predict the electromagnetic scattering from grass blade structures, assuming an incident electric field of arbitrary direction and polarization. To solve this problem, the scattering formulation described by Sarabandi and Senior [5] shall be followed, a formulation which predicts the scattering from long, thin dielectric cylinders of arbitrary cross section.

Initially, the grass blade is assumed to be infinite in length, eliminating the z dependence of the scattered field and essentially reducing the scattering formulation to a two-dimensional problem involving only the grass blade cross section. If, in addition, the blade cross section is electrically small, the scattering formulation can be further reduced by employing the low frequency or Rayleigh approximation, wherein the higher order terms of the wave number k_0 are ignored [2], [8]. Thus, the Rayleigh approximation essentially reduces the scattering formulation to an electrostatics problem within the region of the blade cross section.

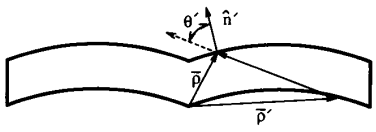

Fig. 2. Cross section of grass blade showing the source point $\bar{\rho}$, the observation point $\bar{\rho}'$, and angle $\theta' = \cos^{-1}[\hat{n}' \cdot (\bar{\rho} - \bar{\rho}')/|\bar{\rho} - \bar{\rho}'|]$.

The expression for the incident electric field after employing the Rayleigh approximation (zeroth order of k_0) is given as

$$\boldsymbol{E}^i = \hat{a} = a_x\hat{x} + a_y\hat{y} + a_z\hat{z} \tag{1}$$

which can be written in terms of the electrostatic potential Φ as

$$\boldsymbol{E}^i = -\nabla_t\Phi^i + a_z\hat{z} \tag{2}$$

where

$$\Phi^i = -a_x(x + c_1) - a_y(y + c_2). \tag{3}$$

Using superposition, the total (incident plus scattered) electrostatic potential can be written as

$$\Phi = a_x\Phi_1 + a_y\Phi_2 \tag{4}$$

where Φ_1 is the total electrostatic potential due to the fist term of (3), and similarly Φ_2 due to the second term.

As shown by Sarabandi and Senior [5], the integral equations specifying the two solutions, Φ_1 and Φ_2, about the outer surface of the blade are given as

$$\left(\frac{\epsilon_r + 1}{2}\right)\Phi_1(\bar{\rho}) - \left(\frac{\epsilon_r - 1}{2\pi}\right)\int_C \Phi_1(\bar{\rho}')\frac{\cos\theta'}{|\bar{\rho} - \bar{\rho}'|}\mathrm{d}c' = -x - c_1 \tag{5}$$

and

$$\left(\frac{\epsilon_r + 1}{2}\right)\Phi_2(\bar{\rho}) - \left(\frac{\epsilon_r - 1}{2\pi}\right)\int_C \Phi_2(\bar{\rho}')\frac{\cos\theta'}{|\bar{\rho} - \bar{\rho}'|}\mathrm{d}c' = -y - c_2 \tag{6}$$

where c_1 and c_2 are arbitrary constants and θ' is defined in Fig. 2.

These equations can be solved using the method of moments, thus determining the total electrostatic potential on the surface of the grass blade. However, this potential must now be related to the scattered electric field. As the scattered field from a nonmagnetic Rayleigh scatterer can be attributed to an electric dipole moment, the scattered field from an infinite Rayleigh cylinder can be attributed to electric dipoles along the infinite (z) axis, expressed as a dipole moment per unit length. The magnitude and direction of this dipole moment is related to the incident electric field vector as $\boldsymbol{p} = \epsilon_0\boldsymbol{P}\cdot\hat{a}$, where $\boldsymbol{P}$ is the polarizability tensor [1], [2] . Because the assumed

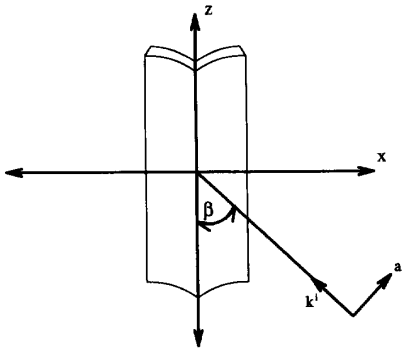

Fig. 3. Geometry of a finite grass blade including incident angle β.

grass blade cross section is symmetrical about the y-axis, the polarizability tensor is a diagonal matrix, and the three nonzero diagonal elements are given as [5]

$$P_{xx} = -(\epsilon - 1)\int_C \Phi_1 \hat{n}' \cdot \hat{x}\mathrm{d}c' \tag{7}$$

$$P_{yy} = -(\epsilon - 1)\int_C \Phi_2 \hat{n}' \cdot \hat{y}\mathrm{d}c' \tag{8}$$

$$P_{zz} = (\epsilon - 1)A. \tag{9}$$

It is important to note that these expressions specifying the polarizability tensor are dependent on only the dielectric constant and geometry of the grass blade. The direction and polarization of the incident electric field does not affect the values of the polarizability tensor, and enter into the scattering formulation only when computing the electric dipole moment ($\boldsymbol{p} = \epsilon_0 \boldsymbol{P} \cdot \hat{a}$).

As stated earlier, this solution was derived assuming an infinite length grass blade. Obviously this is a nonphysical assumption, and to determine the scattered field from a finite blade of length l, the physical optics approximation is employed [4], [8]. The fields on the blade surface calculated for the infinite case (constant with z) are likewise assumed to be valid for the long but finite blade. Integration of these truncated fields along the z axis leads to the familiar $(\sin x)/x$ scattering response in the elevation plane of the blade structure. The scattering intensities are thus given by the expressions [5]

$$\boldsymbol{S} = -\frac{k_0^2}{4\pi}\left\{\hat{k}^s \times \hat{k}^s \times [l\boldsymbol{P} \cdot \hat{a}]\right\}\frac{\sin U}{U} \tag{10}$$

where

$$U = \frac{k_0 l}{2}\left(\hat{k}^s \cdot \hat{z} - \cos\beta\right), \tag{11}$$

with $\boldsymbol{P}$ being the polarizability tensor given by (7)–(9), l the blade length, and β the incident angle in the elevation plane, as defined in Fig. 3. Fig. 4(a) displays a typical scattering pattern in the elevation plane, with the main lobe occurring at the forward scattering cone. Although this physical optics formulation is merely an approximation, it can predict the major scattering behavior for blades with electrical lengths as small as one λ, although accuracy generally increases with cylinder electrical length.

In the azimuth plane, the scattering response (Fig. 4(b)) is that of an electric dipole, as expected for electrically small

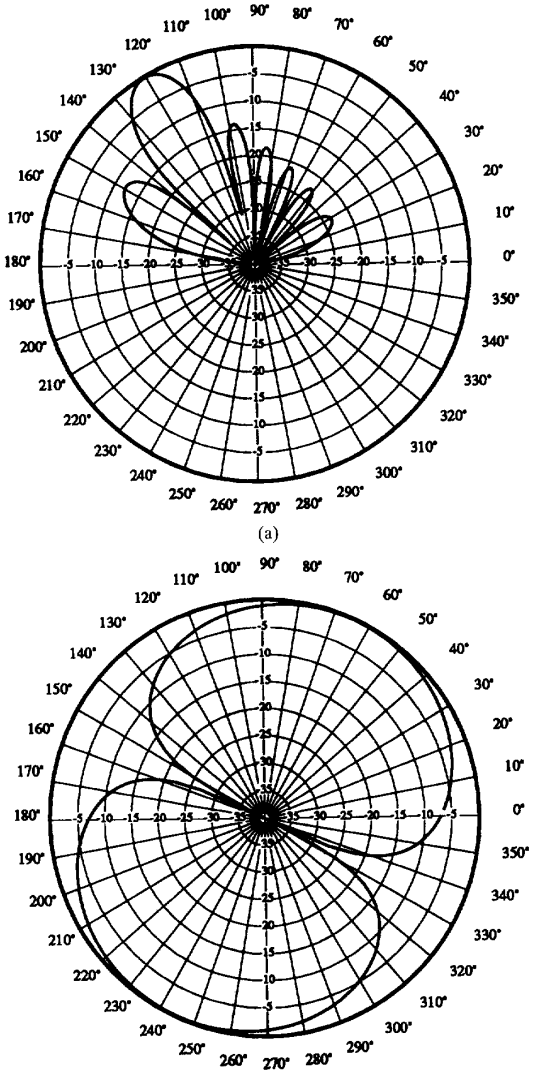

(a)

(b)

Fig. 4. Scattered intensity in the elevation (a) and azimuth (b) planes of a horizontally polarized wave incident on a finite dielectric cylinder ($\theta_i = 60°, \phi_i = 45°$, $l = 2\lambda$, $P_{xx} = 4.0$, $P_{yy} = 2.0$).

(Rayleigh) cross sections. It should be noted, however, that except for the specific case of $P_{xx} = P_{yy}$, the radial electric dipole moment will not align with the incident electric field vector. Thus, the main forward and backscattering lobes will not be aligned with the radial direction of the incident field propagation vector.

To validate this scattering formulation, the backscattering coefficient is determined as a function ofelevation angle using an accurate three-dimensional numeric scattering model. If $\theta = 0$ and $v = 0$, the grass blade shape reduces to a flat dielectric strip. A flat, thin dielectric structure can be modeled as a resistive sheet [13], [14], and therefore the grass blade in this case is modeled as a resistive strip. Using a moment-method code which provides a scattering solution

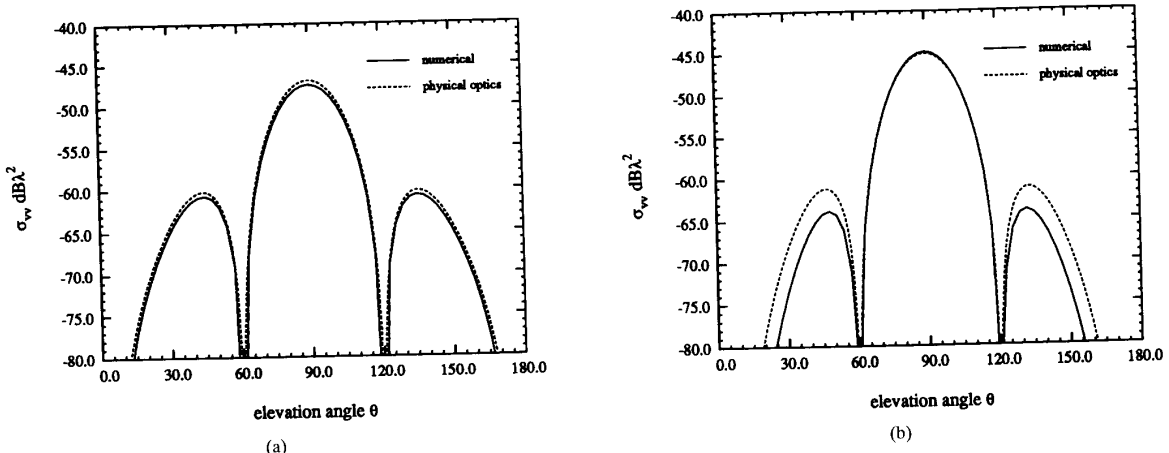

Fig. 5. Normalized backscattering rcs σ_{hh} (a) and σ_{vv} (b) as determined by both a numeric scattering model and the scattering formulation of this paper. ($\phi = \pi/2$ $a = 0.05$ $\theta = v = 0, \epsilon = 5 - i1, A = 1.25 \times 10^{-4}\lambda^2, l = \lambda$).

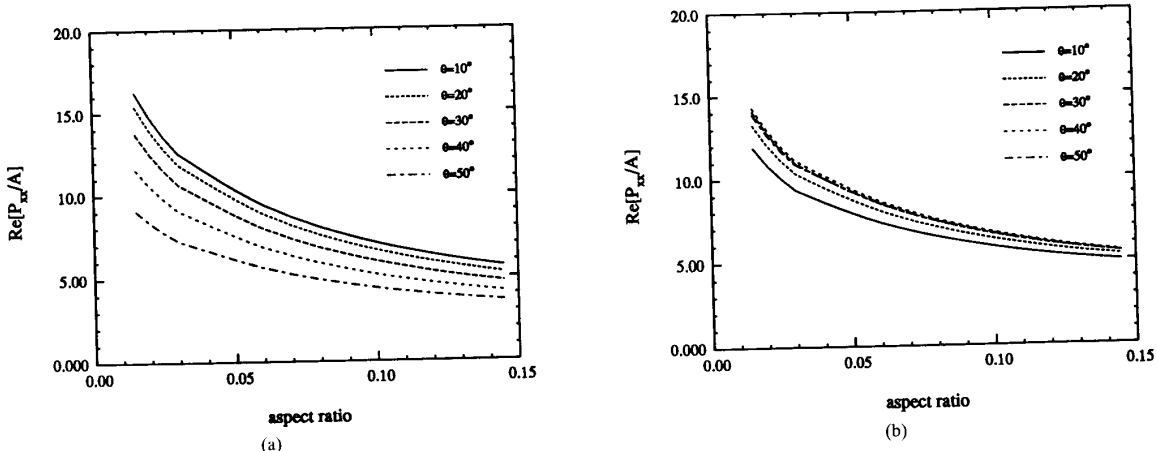

Fig. 6. The real portion of the normalized polarizability tensor element P_{xx}/A as a function of aspect ratio a and blade angle θ for blade curvature v =(a) 0.2 and (b) 1.5 ($\epsilon = 30 + j9$).

for an arbitrary resistive sheet, the backscattering coefficient σ versus elevation angle was calculated and the results are given in Fig. 5, along with the data predicted by (10) using the polarizabity tensor. Good agreement between the two methods was found, with an error for σ_{hh} of less than 1 dB for all incidence angles. The error for σ_{vv} is similar when close to normal incidence, but becomes larger with increasing oblique incidence as traveling waves (not accounted for in the physical optics approximation) are induced. However, the cylinder of Fig. 5 is just one λ in length, and the error at large oblique angles diminishes as cylinder length increases.

IV. Model Results

The effect of blade geometry on scattering from grass blades was evaluated using the scattering formulation outlined in the previous section. The parameter of interest in this case is the normalized polarizability tensor $\boldsymbol{P}/A$. Each element of the polarizability tensor is directly proportional to the cross-section area A, thus the normalized polarizability tensor $\boldsymbol{P}/A$ is independent of A. Therefore, $\boldsymbol{P}/A$ is a function of only the dielectric constant and the shape, as described by the dimensionless shape parameters, curvature v, aspect ratio a, and blade angle θ. In general, the elements P_{xx} and P_{yy} are, respectively, proportional to the projected area of the blade shape onto the (x, z) and (y, z) planes. Thus, the parameter which most affects the normalized polarizability tensor elements is aspect ratio, followed by blade angle and then blade curvature. Fig. 6 demonstrates this dependence, showing the effect of aspect ratio and blade angle on the real part of P_{xx}/A for both a relatively flat and a relatively curved grass blade geometry.

Although these figures demonstrate the dependence of polarizability tensor, and hence scattering on blade geometry, the larger question of whether these shape parameters significantly affect scattering from an entire grassland target can not be inferred. Therefore, a radiative transfer scattering model [9]–[11] was implemented which modeled a layer of scatterers consisting of cylinders of a given length and cross-sectional

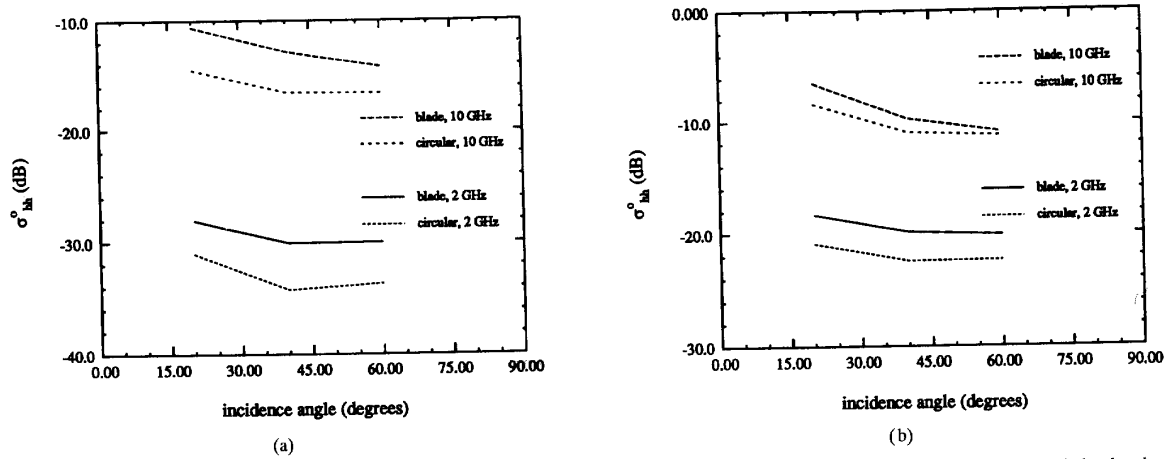

Fig. 7. σ°_{hh} for dry (a) and moist (b) vegetation as predicted by a radiative transfer based grassland model for blades of both grass blade and circular shaped cross sections ($a = 0.45$, $\theta = 0$, $v = 0.01$, $N = 2500/\mathrm{m}^3, l = .5$ m, $A = .03$ cm^2, $M_g = 0.3$ (a) and 0.9 (b)).

area. Two cases were examined; in the first case, the cylinders were of circular cross section, while in the other a blade shaped cross section ($a = 0.045$, $\theta = 0$, $v = 0.01$) of identical area was implemented. Fig. 7 displays the results of this model at two frequencies for two dielectric constants and three incidence angles. The difference in the cross-section shape results in a difference of as much as 5 dB in the value of σ°_{hh}. This contrast is largest at lower frequencies and for drier grass blades. Although this data represents a limited test case, it does show that for electrically small cross sections, blade shape, in addition to blade size, *can* significantly affect the observed scattering from grassland targets.

V. Algebraic Model

For a cylinder of circular cross section, an exact analytic solution to the integral equations of (5) and (6) exists, thus leading to an exact solution of the normalized polarizability tensor elements as a function of the complex dielectric constant [5], [8]:

$$\frac{P_{xx}}{A} = \frac{P_{yy}}{A} = 2\frac{\epsilon - 1}{\epsilon + 1}. \tag{12}$$

As shown by Sarabandi and Senior [5], this equation can be modified to provide an approximate algebraic solution for cylinders of semi-circular, triangular, and square cross sections which, although not an exact solution to the integral equations, matches the numeric solution with exceptional accuracy. This modified expression is given as

$$\frac{P(\epsilon)}{A} = c_0 \frac{\epsilon - 1}{\epsilon + 1} \cdot \frac{\epsilon + c_1}{\epsilon + c_2} \tag{13}$$

where the values of constants c_0, c_1, and c_2 are unique for each of the three cross sections. This expression is valid for both P_{xx}/A and P_{yy}/A, although the three constants are of course different for nonsymmetric cross sections (semicircular and triangular).

To determine if the validity of this expression extends to grass blade shapes, data was generated with the numerical model for a given blade geometry across a wide range of complex dielectric constants. Three constants c_1, c_2, and c_3 were then selected in an attempt to match (13) to the generated numerical data. As shown in Fig. 8, constants were found which provided a match with good accuracy between the approximation of (13) and the numerical data. Thus, (13) appears to be valid for not only simple geometrical cross sections, but for more general cross sections (grass blades) as well. The constants c_0, c_1, and c_2, denoted as vector $\boldsymbol{c}$, can therefore be selected to relate the dielectric constant to the polarizability tensor for a given blade geometry. Since these constants are dependent only on cross-section geometry, and since cross-section geometry for a grass blade has been defined by the three shape parameters v, a, and θ, a more general algebraic approximation relating grass blade geometry, in addition to the dielectric constant, can be hypothesized:

$$\frac{P_{xx}}{A} = c_0(\theta, a, v)\frac{\epsilon - 1}{\epsilon + 1} \cdot \frac{\epsilon + c_1(\theta, a, v)}{\epsilon + c_2(\theta, a, v)}. \tag{14}$$

The expressions relating $\boldsymbol{c}$ to the shape parameters v, a, and θ must therefore be determined.

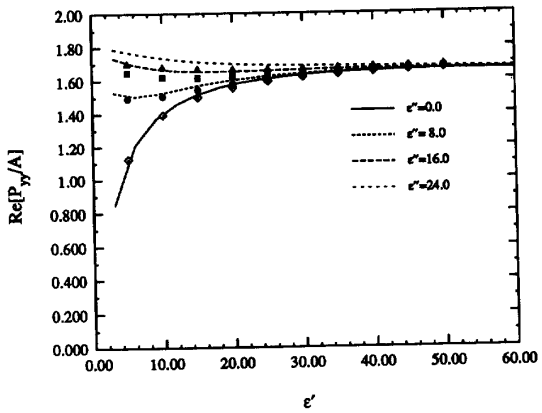

Fig. 8. Comparison of the predicted dependence of Re$[P_{yy}/A]$ on dielectric constant for both the numerical scattering model (lines) and the algebraic approximation (marks) of (13) ($a = 0.1$, $\theta = 28°$, $v = 0.01$, $c_0 = 1.753$, $c_1 = 9.703$, and $c_2 = 10.297$).

TABLE II
MODEL INPUT PARAMETER SPACE ESTIMATING THOSE VALUES GENERALLY OBSERVED IN NATURE

parameter	min.	max.
aspect ratio (a)	0.015	0.12
blade angle (θ)	0.0	50.0
curvature (v)	0.01	2.0
dielectric constant (ϵ')	5.0	45.0
dielectric constant (ϵ'')	2	25

VI. COEFFICIENT ESTIMATION

To determine these relationships, the numerical model was used to determine the normalized polarizability tensor $\boldsymbol{P}/A$ for various dielectrics for each of 512 separate blade geometries. These 512 geometries were uniformly selected from the parameter space shown in Table II, describing the limited domain of geometries and dielectrics which, in general, are observed for grass blades. For a given geometry, six constants c_n must be determined, three for each P_{xx}/A and P_{yy}/A. Using the results of the numerical model at three distinct dielectric constants, a non-linear system of three equations ($\boldsymbol{P}(\epsilon_1)/A$, $\boldsymbol{P}(\epsilon_2)/A$, $\boldsymbol{P}(\epsilon_3)/A$) with three unknowns ($c_1$, c_2, c_3) is formed using (13). Thus, nonlinear inversion techniques can be used to determine the three elements of $\boldsymbol{c}$ [3, ch. 9]. However, because (13) is merely an approximation, and not an exact solution for $\boldsymbol{P}/A$, inversion techniques may lead to erroneous results. Inversion techniques force a solution which produces zero error at each of the three data points $\boldsymbol{P}(\epsilon_1)/A$, $\boldsymbol{P}(\epsilon_2)/A$, and $\boldsymbol{P}(\epsilon_3)/A$, however, in so doing may severely affect the accuracy of the approximation at other dielectric constant values.

As an alternative solution, the polarizability tensor elements were numerically computed at additional dielectric constants (six were found to be sufficient), and the three coefficients of $\boldsymbol{c}$ were then determined by locating those values which minimized the sum of the squared errors between (13) and the numerical data at these six dielectric values. Although the resulting algebraic approximation may exhibit nonzero error at all six dielectric values, the solution does match the numerical model results across the entire range of dielectric values. To determine an optimum selection of the vector $\boldsymbol{c}$, the conjugate gradient technique [3, ch. 10] was implemented which iteratively converges to the values of c_1, c_2, and c_3 that minimize the total squared error equation:

$$\sum_{n=1}^{6}\left(P_{num}(\epsilon_n)/A - c_0\frac{\epsilon_n-1}{\epsilon_n+1}\cdot\frac{\epsilon_n+c_1}{\epsilon_n+c_2}\right)^2, \qquad (15)$$

where $P_{num}(\epsilon_n)/A$ is the polarizability tensor element of a specified blade geometry with dielectric ϵ_n, as determined by the numerical model. Fig. 9 contrasts the difference in the solutions obtained by using both an inversion and a minimization technique on the same set of numerical data. The minimization (conjugate gradient) technique selects coefficients $\boldsymbol{c}$ which result in a model matching all the numeric data points, whereas the inversion (Newton–Raphson) method results in a range of dielectric constants where (13) produces erroneous values for $\boldsymbol{P}/A$.

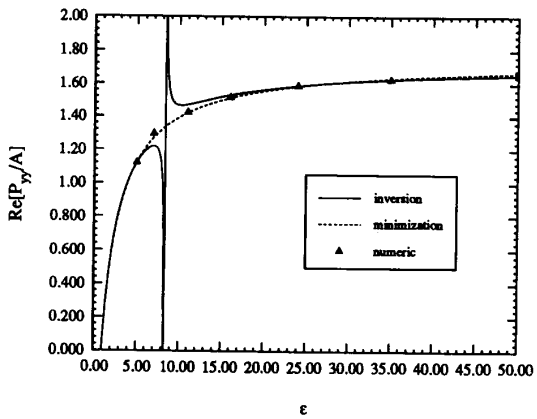

Fig. 9 . Re$[P_{yy}/A]$ versus ϵ as predicted by (13) using coefficients $\boldsymbol{c}$ determined by both inversion and error minimization methods. The inversion method results in large errors for some values of ϵ.

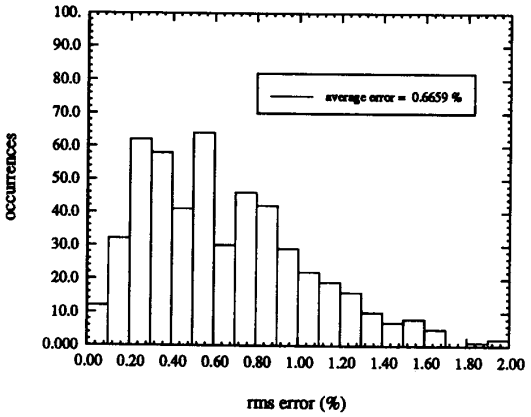

Fig. 10. Histogram showing the distribution of the average rms error resulting from the approximation of (13) determined at 512 test geometries. The coefficients $\boldsymbol{c}$ were selected using a conjugate gradient error minimization technique.

Therefore, the conjugate gradient method was implemented on the selected 512 geometries to provide two sets of vector $\boldsymbol{c}$ (one set for each P_{xx}/A and P_{yy}/A) for each of the 512 cases. Fig. 10 shows a histogram over the 512 geometries of the average rms error between the numerical model and the analytic approximation, using the coefficients as selected by the conjugate gradient technique. The average error for P_{xx}/A was 0.07%, whereas the average error for P_{yy}/A was determined to be approximately 0.7 %. For each of the 512 geometries, a set of constants was found which provided an accurate model of the relationship between the dielectric constant and the polarizability tensor.

The conjugate gradient method converges to a set of coefficients $\boldsymbol{c}$ which provide a model with a minimum total

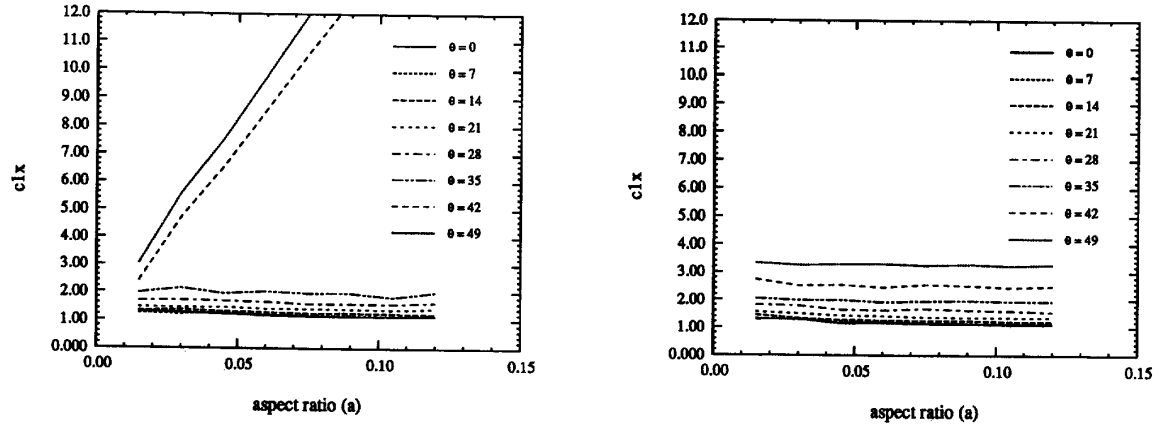

Fig. 11. Two valid solutions for constant c_1 (of P_{xx}/A) versus aspect ratio and blade angle; a dual-mode solution (a) resulting in a discontinuous function of c_1 versus θ, and a single-mode solution (b) resulting in a continuous function of c_1.

squared error. However, this minimum may not be the global minimum, as the conjugate gradient may converge to any number of local minima, depending on the initial value of $\boldsymbol{c}$ used by the conjugate gradient routine. These minima can be thought of as different "modes," with each mode producing a slightly different curve for (13), each matching the six numerical data points $(P_{num}(\epsilon_n)/A)$ in a slightly different fashion. For instance, one mode may result in a model which slightly underestimates the first three data points $P(\epsilon)/A$ and slightly overestimates the last three, whereas for another mode the reverse may be true. Many of these modes may produce acceptable accuracy, but the desired solution is the mode associated with the smallest error (the global minimum). However, the mode associated with the global minimum at one geometry may not be the mode corresponding to the global minimum at another. Since we are ultimately seeking an expression relating c_1, c_2, and c_3 to the shape parameters v, a, and θ, a solution involving a single mode is required to avoid discontinuities in $\boldsymbol{c}$ across the domain of Table II. For example, Fig. 11(a) shows a solution for constant c_1 versus aspect ratio for various blade angle values. For blade angle values from $\theta = 0°$ to $\theta = 35°$, the minimum is associated with a single mode, however for $\theta = 42°$ and $49°$ the conjugate gradient algorithm converges to a different minimum, resulting in significantly different data and a large discontinuity in c_1 versus θ. Fig. 11(b) shows the single-mode solution, a solution which is well behaved and continuous across both aspect ratio and blade angle.

If, for various regions of the blade shape parameter space (Table II), the global minimum is associated with separate modes, then the selection of the "optimum" mode becomes a compromise between minimizing the average error across the parameter space and minimizing the maximum error occurring at any given point. In addition, forcing the conjugate gradient routine to converge to the same mode for all blade geometries may also prove to be difficult, as mode selection is determined only by the initial value of $\boldsymbol{c}$ of the conjugate gradient algorithm. This initial value must be "close" enough to the correct solution for the conjugate gradient method to converge to that minimum rather than to another. Since the correct solution is unknown, selection of the initial values of $\boldsymbol{c}$ for a given geometry is problematic. Often several trials were required to force the conjugate gradient to converge to the correct mode. However, as $\boldsymbol{c}$ was determined for a significant number of blade geometries, an approximate relationship between the elements of $\boldsymbol{c}$ and the shape parameters v, a, and θ was inferred, and then used to properly determine an initial value for a given geometry.

VII. Polynomial Fit

Once a single-mode solution for $\boldsymbol{c}$ for both P_{xx} and P_{yy} was determined for all 512 sample geometries, the mapping between $\boldsymbol{c}$ and the shape parameters v, a, and θ, could be replaced with a polynomial expression used to estimate the values of $\boldsymbol{c}$ across the domain of Table II. These polynomials can then be used in (14) to provide a complete algebraic approximation of the numerical scattering formulation of Section III.

To match a polynomial approximation to the data $\boldsymbol{c}$, a solution is assumed which is a linear combination of M basis functions, each basis function being an expression involving the parameters v, a, and θ. The number of basis functions is a compromise between the complexity and accuracy of the polynomial approximation, and for this application a third-order expansion consisting of 20 basis functions was chosen. For the polynomials associated with the normalized polarizability tensor P_{xx}/A, the basis functions (as determined by trial and error) are expansions of the parameters v, $(1/a)$, and $\cos\theta$; the general polynomial approximations for $\boldsymbol{c}$ are therefore given as

$$c_n = \sum_{i=0}^{3}\sum_{j=0}^{3}\sum_{k=0}^{3} b_m \frac{\mathrm{v}^i \cos^j\theta}{\mathrm{a}^k}, \tag{16}$$

such that $i + j + k \leq 3$, $m = 1, 20$, and $n = 1, 3$. For the polynomials of P_{yy}/A, the chosen basis functions are an expansion of the parameters v, $(1/a)$, and $\sec\theta$, thus the

TABLE III
VALUES OF THE 20 COEFFICIENTS b_m FOR EACH OF THE SIX EXPANSIONS OF c, AS GIVEN BY (17) AND (18)

		$\mathbf{P}_{xx}/A$			$\mathbf{P}_{yy}/A$		
i,j,k	b_m	c_0	c_1	c_2	c_0	c_1	c_2
0,0,0	b_1	-11.18	13.29	17.82	-12.94	28.02	-9.268
0,0,1	b_2	-0.8747	-3.469E-02	1.769	0.2781	9.4470E-03	-0.2167
0,0,2	b_3	-1.307E-02	-3.569E-05	-1.466E-02	-1.768E-03	2.574E-03	-4.961E-03
0,0,3	b_4	1.031E-04	-1.287E-06	1.108E-04	1.253E-05	-1.111E-05	5.296E-05
0,1,0	b_5	50.81	-24.15	-49.43	16.92	-16.94	21.39
0,1,1	b_6	3.444	9.537E-02	-1.197	-0.491	-5.920E-02	0.595
0,1,2	b_7	5.384E-04	1.068E-04	8.748E-04	4.137E-04	-1.204E-03	-1.098E-03
0,2,0	b_8	-85.25	15.15	44.45	-0.9688	-2.717	-4.099
0,2,1	b_9	-1.611	-5.654E-02	0.5463	0.2635	-2.507E-02	-0.1640
0,3,0	b_{10}	46.74	-3.199	-13.91	-2.435	3.558	-1.006
1,0,0	b_{11}	-10.16	-0.3726	-7.273	24.61	-38.03	38.43
1,0,1	b_{12}	0.5911	2.250E-02	-0.3542	0.1876	-0.2218	6.614E-02
1,0,2	b_{13}	6.520E-04	-4.893E-06	5.482E-04	-1.720E-04	7.368E-04	1.796E-04
1,1,0	b_{14}	42.69	-8.406	-1.913	-37.74	55.67	-54.33
1,1,1	b_{15}	-0.6183	-2.045E-02	0.2870	-0.1915	0.1518	-5.175E-02
1,2,0	b_{16}	-31.18	8.512	10.01	12.74	-16.36	15.16
2,0,0	b_{17}	-3.462	0.6613	6.350	-0.5466	1.895	-1.887
2,0,1	b_{18}	-6.594E-02	-3.032E-03	5.077E-02	3.487E-02	-1.413E-02	-2.532E-03
2,1,0	b_{19}	2.133	-5.807E-02	-4.617	1.855	-4.746	5.115
3,0,0	b_{20}	0.2449	4.645E-02	-0.5782	-0.3788	0.7839	-0.9007

polynomials are given as

$$c_n = \sum_{i=0}^{3}\sum_{j=0}^{3}\sum_{k=0}^{3} b_m \frac{\mathrm{v}^i \sec^j \theta}{\mathrm{a}^k}, \tag{17}$$

such that $i + j + k \leq 3$, $m = 1, 20$, and $n = 1, 3$.

Using orthogonality principles, the values of the coefficients b_m are determined by solving the linear estimation equation [3, ch. 141]

$$(X^T \cdot X) \cdot b = X^T \cdot C \tag{18}$$

where $\boldsymbol{b}$ is a 20 element vector containing the polynomial coefficients, $\boldsymbol{C}$ is a 512 element vector containing the conjugate gradient estimate of c_n at the 512 test geometries, and $\boldsymbol{X}$ is a 512 $\times$ 20 matrix containing rows of the 20 basis functions evaluated at the 512 test geometries. The coefficients $\boldsymbol{b}$ determined by this computation are given in Table III. Thus, (14), (16), and (17), along with the coefficients listed in Table III, provide a fast algebraic approximation to the slower numerical model of Section III.

VIII. RESULTS

To test the accuracy of this algebraic approximation, 3125 test points, covering the range of shape parameters and complex dielectric constants found in Table II, were selected and used to determine the complex elements of the polarizability tensor with both the numerical model and the algebraic approximation. The magnitude of the vector formed by P_{xx} and P_{yy}, defined as:

$$|P| = \sqrt{P_{xx}P_{xx}^* + P_{yy}P_{yy}^*}, \tag{19}$$

was calculated for both models, and this data was used to build the histogram of Fig. 12, showing the percent error

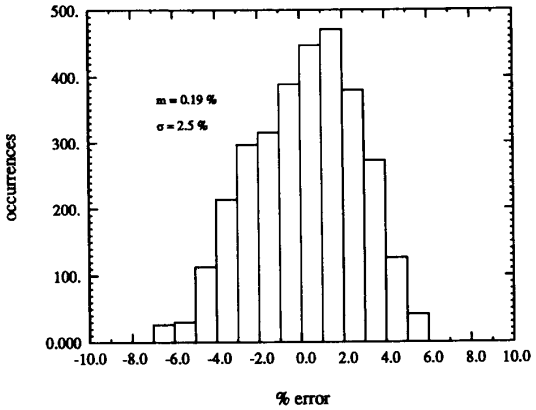

Fig. 12. Histogram showing the distribution of the error resulting from the approximation given by (14), as determined using 3125 test cases covering the range of parameters given in Table II.

of the algebraic approximation of $|P|$ as compared to the numerical model. As estimated from 3125 test cases, the algebraic approximation exhibited little bias, with a mean error of 0.2%, in addition to producing an acceptable rms error of 2.5%. Fig. 13 shows the accuracy typical of the approximation, displaying the predictions of both the numeric and algebraic models for Re$[P_{xx}/A]$ versus aspect ratio at a number of blade angle values.

IX. CONCLUSIONS

Using a numerical solution to solve the scattering problem of cylinders with arbitrary cross sections, it was determined that blade shape, in addition to blade size, can significantly affect the scattering solution for a long, thin grass blade structure. Likewise, a simple radiative-transfer model demonstrates

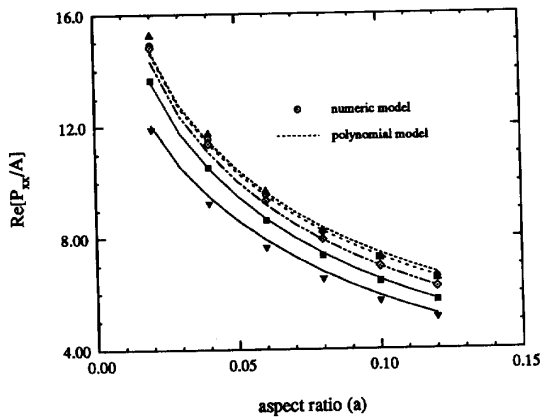

Fig. 13. Comparison of the polynomial approximation to the numerical model predictions for Re$[P_{xx}/A]$ versus aspect ratio at various blade angles.

that the calculated backscattering coefficients for grassland target can also be significantly affected. The numerical scattering model is required for characterizing scattering by complex grass blade shapes. However, direct implementation of this numerical model into a larger radiative-transfer solution for grassland targets can result in a model of unacceptable computation time and complexity, especially when the radiative-transfer model is used in an inversion algorithm.

Although the complexity of the numerical model is necessary to describe a cylinder of arbitrary cross section, the cross sections associated with grass blades are not arbitrary but are instead limited to those described by parameters a, v, and θ, and by the domain of Table II. These limits greatly reduce the information requirement of the numerical scattering model, thereby allowing for its replacement by a relatively simple analytical approximation. By combining the relationship of $\boldsymbol{P}/A$ with ϵ (13) and the relationship of $\boldsymbol{c}$ versus a, v, and θ inferred from a small but representative sample of numeric solutions (16), (17), an analytic approximation was developed that can predict the scattering response of blade shaped cylinders both rapidly and accurately.

REFERENCES

[1] J. B. Keller, R. E. Kleinman, and T. B. A. Senior, "Dipole moments in Rayleigh scattering," *J. Inst. Math. Appl.*, vol. 9, pp. 14–22, 1972.

[2] R. E. Kleinman and T.B.A. Senior, "Rayleigh scattering," in *Low and High Frequency Asymptotics*, V. K. Vardan and V. V. Vardan, Eds. Amsterdam: North-Holland, 1986, pp. 1–70.

[3] W. H. Press, *Numerical Recipes*. Cambridge: Cambridge University Press, 1989.

[4] G. T. Ruck, D. E. Barrick, W. D. Stuart, and C. K. Krichbaum, *Radar Cross Section Handbook*,, vol. 1. New York: Plenum Press, 1970.

[5] K. Sarabandi and T. B. A Senior, "Low-frequency scattering from cylindrical structures at oblique incidence," *IEEE Trans. Geosci. Remote Sensing*, vol. 28, no. 5, pp. 879–885, 1990.

[6] K. Sarabandi, T. B. A. Senior, and F. T. Ulaby, "Effect of curvature on the backscattering from a leaf," *J. Electromag. Waves Appl.*, pp. 653–670, 1988.

[7] K. Sarabandi and F.T. Ulaby, "High frequency scattering from corrugated stratified cylinders'," *IEEE Trans. Antennas Propagat.*, vol. 39, pp. 512–520, Apr. 1991.

[8] T.B.A. Senior, and K. Sarabandi, "Scattering models for point targets," in *Radar Polarimetry for Geoscience Applications*, F.T. Ulaby and C. Elachi, Eds. Norwood, MA: Artech House, 1990.

[9] L. Tsang, J. A. Kong, and R. T. Shin, *Theory of Microwave Remote Sensing*. New York: Wiley, 1985, chapter 3.

[10] Y. Kuga, M. W. Whitt, K. C. McDonald, and F. T. Ulaby, "Scattering models for distributed targets," in *Radar Polarimetry for Geoscience Applications*, F.T. Ulaby and C. Elachi, Eds. Norwood, MA: Artech House, 1990.

[11] F. T. Ulaby, R. K. Moore, and A. K. Fung, *Microwave Remote Sensing: Active and Passive*. Norwood, MA: Artech House, 1981, chapter 13.

[12] F. T. Ulaby, K. Sarabandi, K. McDonald, M. Whitt, and M. C. Dobson, "Michigan microwave canopy scattering model," *Int. J. Remote Sensing*, vol. 11, no. 7, pp. 1223–1253, 1990.

[13] M. I. Herman and J. L. Volakis, "High-frequency scattering by a resistive strip and extensions to conductive and impedance strips," *Radio Sci.*, vol. 22, no. 3, pp. 335–349, 1987.

[14] R. F. Harrington and J. R. Mautz, "An impedance sheet approximation for thin dielectric shells," *IEEE Trans. Antennas Propag.*, vol. AP-25, pp. 531–534, 1975.

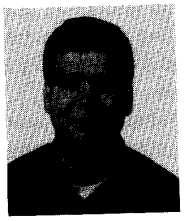

James M. Stiles was born in Kansas City, MO, in 1961. He received the B.S.E.E. degree from the University of Missouri in 1983, and the M.S.E.E. degree from Southern Methodist University in 1987. He is presently pursuing the Ph.D. degree in electrical engineering at the University of Michigan.

From 1983 to 1990 he was an RF Design Engineer for Texas Instruments Inc., Dallas, TX. His interest include electromagnetic scattering from vegetation and application of estimation theory to microwave remote sensing.

Kamal Sarabandi (S'87–M'90–SM'93) received the B.S. degree in electrical engineering from Sharif University of Technology, Tehran, Iran, in 1980, the M.S.E. degree in electrical engineering in 1986, and the M.S. degree in mathematics and the Ph.D. degree in electrical engineering in 1989, all three from the University of Michigan.

From 1980 to 1984 he worked as a Microwave Engineer in the Telecommunication Research Center in Iran. He is presently an Assistant Professor in the Department of Electrical Engineering and Computer Science at the University of Michigan. His research interests inlcude elctromagnetic scattering, microwave and milimeter wave remote sensing, and calibration of polarimetric SAR systems.

Dr. Sarabandi is a member of the Electromagnetics Academy and USNC/URSI Commission F.

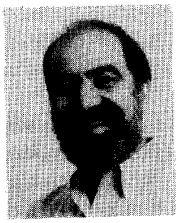

Fawwaz T. Ulaby (M'68–SM'74–F'80) received the B.S. degree in physics from the American University of Beirut, Lebanon, in 1964 and the M.S.E.E. and Ph.D. degrees in electrical engineering from the University of Texas, Austin, in 1966 and 1968, respectively.

He is currently Professor of Electrical Engineering and Computer Science at the University of Michigan, Ann Arbor, and Director of the NASA Center for Space Terahertz Technology. His current interests include microwave and millimeter wave remote sensing, radar systems, and radio wave propagation. He has authored several books and published over 400 papers and reports on these subjects.

Dr. Ulaby has received numerous awards, inluding the IEEE Geoscience and Remote Sensing Distinguished Achievement Award in 1983, the IEEE Centennial Medal in 1984, and the Kuwait Prize in Applied Science in 1986.